Fusion Engineering and Design 23 (1993) 115–132
North-Holland

Thermal-hydraulic and structural design of the TITAN-I reversed-field-pinch fusion power core

Mohammad Z. Hasan, Nasr M. Ghoniem, James P. Blanchard * and the TITAN Team **

Institute of Plasma and Fusion Research, University of California, Los Angeles, CA 90024-1597, USA

Thermal-hydraulic and structural design of the first wall, blanket, and shield of the deuterium–tritium fueled TITAN-I reversed-field-pinch (RFP) fusion reactor is presented. Taking advantage of the characteristic low toroidal magnetic field of an RFP reactor, liquid lithium is used as the primary coolant to remove the thermal energy at an elevated temperature, thereby realizing a high power conversion efficiency of 44%. The use of liquid lithium has also led to a self-cooled design of the fusion power core in which the primary coolant is also the tritium breeder. The structural material is the vanadium alloy, V–3Ti–1Si. Tubular coolant channels are used in the first wall/blanket and rectangular channels in the hot shield. These are laid along the much larger poloidal field to minimize magnetohydrodynamic (MHD) pressure drop. Although the neutron wall loading of 18.1 MW/m^2 is high, resulting in a radiation heat flux on the first wall of 4.6 MW/m^2, three aspects of the design have made the removal of the reactor power at high temperature possible. These are: (1) the use of small-diameter circular tubes as coolant channels in the first wall, (2) the use of high-velocity MHD turbulent flow in the first-wall coolant tubes, and (3) thermal separation of the first-wall and blanket/shield coolant circuits, thereby allowing different exit temperatures. The thermal-hydraulic design was optimized by a design code developed for this purpose. Detailed structural design was performed by the finite element code ANSYS. The coolant inlet temperature is 320°C, and the coolant exit temperatures for the first-wall and blanket/shield coolant circuits are 442°C and 700°C, respectively. Lithium flow velocity in the first-wall coolant tubes is 21.6 m/s, and is ≤ 50 cm/s in the blanket/shield coolant channels. The total pressure drop in the first-wall coolant circuit is 10 MPa and in the blanket coolant circuit it is 3 MPa. The pumping power for coolant circulation is less than 5% of the net electric output. The material stresses are well within the design limits. The TITAN-I design suggests the feasibility and advantage of liquid-metal cooling of high wall loading RFP fusion reactors.

1. Introduction

TITAN is a conceptual, deuterium–tritium fueled, power reactor based on the reversed-field-pinch (RFP) concept of plasma confinement [1]. For a power reactor, the thermal-hydraulic design is intimately coupled to power conversion and safety. Power conversion efficiency is affected by the coolant inlet and exit temperatures. Safety requirements dictate that the structural temperature, temperature gradient, coolant pressure, and pressure drop be low enough that the design limits on temperature, pumping power, and material stress are not exceeded. The thermal-hydraulic design should also facilitate the removal of decay heat under accident conditions and be favorable to blanket energy multiplication and tritium breeding.

Liquid metals are generally excellent coolants because of their high thermal conductivity and high boiling point. One of their drawbacks, however, is the large pressure drop encountered when they are circulated across magnetic fields. If such magnetohydrodynamic (MHD) pressure drop can be kept low, a liquid-metal coolant will require much lower coolant pressure than a gas coolant. Many studies have proposed or considered liquid lithium as a coolant for fusion reactors [2–7]. In an RFP fusion reactor, such as TITAN, the toroidal magnetic field at the first wall is quite small, thus the MHD pressure drop can be kept low by aligning the coolant channels with the much larger poloidal field. The fusion power core (FPC) of TITAN-I

* *Present address:* University of Wisconsin, Fusion Technology Institute, Madison, WI 53706-1687, USA.

** See p. 69.

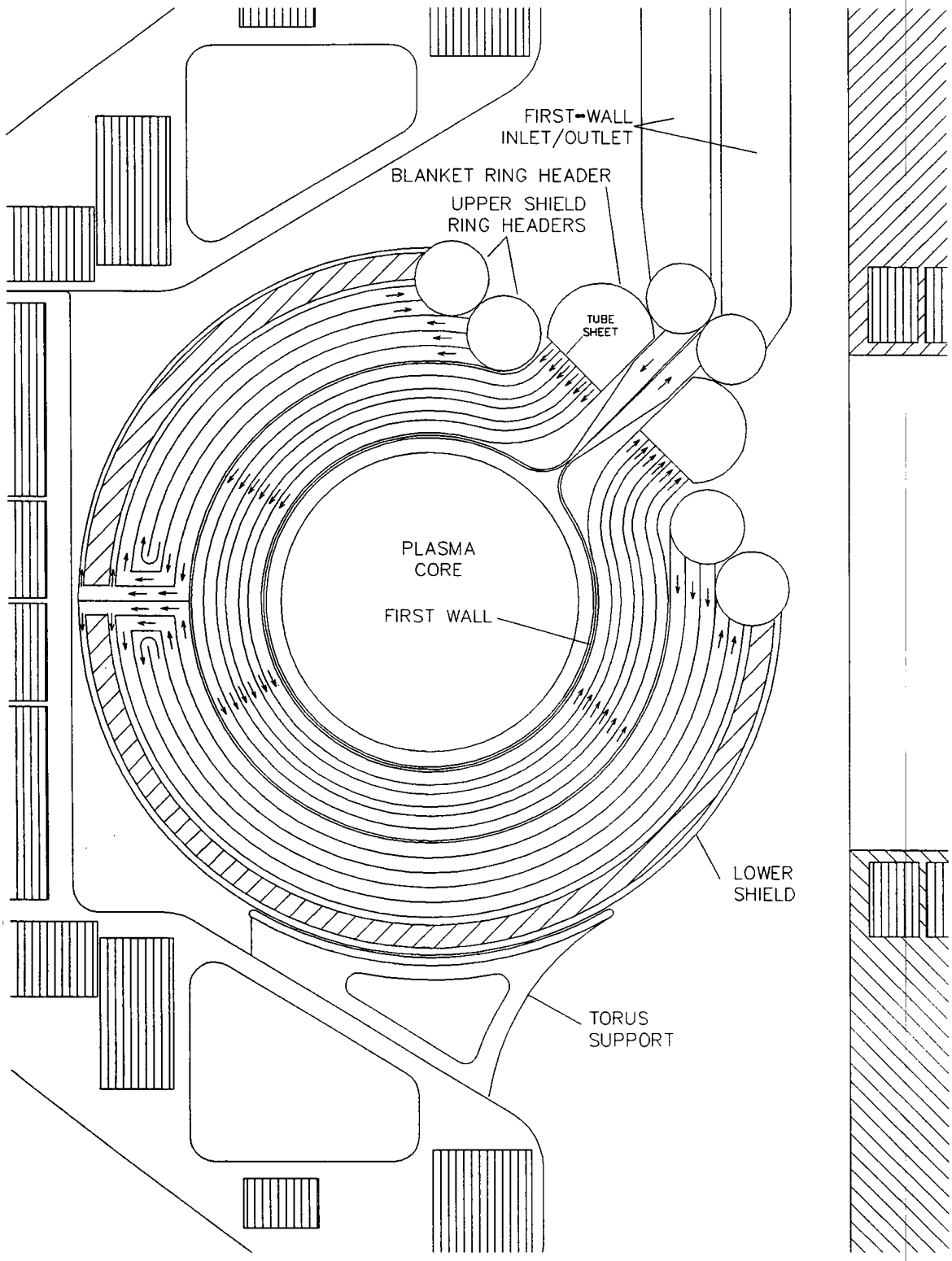
FIRST-WALL
INLET/OUTLET
BLANKET RING HEADER
UPPER SHIELD
RING HEADERS
TUBE
SHEET
PLASMA
CORE
FIRST WALL
LOWER
SHIELD
TORUS
SUPPORT

Table 1
Heat load (MW) on TITAN-I FPC components

Power to first wall	
Surface heating	462.2
Nuclear heating	
Structure	115.9
Coolant	118.1
Pumping power [a]	37.7
Total	735.9
Power to IBC	
Nuclear heating	
Structure	373.3
Coolant	870.1
OFCD joule heating [b]	17.0
TF-IBC joule heating	25.6
Pumping power [a]	6.0
Total [c]	1292.0
Power to hot shield	
Nuclear heating	
Structure	458.9
Coolant	247.3
Pumping power [a]	3.0
Total	709.2

[a] A pump efficiency of 90% is assumed.
[b] Joule heating in the IBC, which is also the toroidal-field driver coil of the OFCD system, and from eddy currents (1 MW).
[c] Excluding 168.8 MW which is deposited in the divertor IBC.

is cooled by liquid lithium; the main reasons are to recover the thermal energy at high temperature and to obtain a compact FPC design through tritium breeding in the primary coolant itself and through the use of an integrated blanket coil (IBC) [8]. In the IBC concept, the primary coolant in the blanket carries electric current to produce the required toroidal magnetic field, thus eliminating the need for external toroidal-field coils.

Table 1 summarizes the heat load on the TITAN-I FPC components. The first wall is exposed to a radiation heat flux of about 4.6 MW/m^2, while in the blanket and hot shield the heat loads result from the volumetric nuclear heating. Tubular coolant channels with circular cross section are suitable for the first wall, since a channel with circular cross section has higher heat-transfer capability (Nusselt number) and lower induced stresses compared with other geometries. The requirements of heat-transfer capability and material strength for the blanket-coolant channels are less stringent because of much smaller heat loads and coolant velocities.

The geometry, size, and configuration of the coolant channels are important parameters in thermal-hydraulic design. Figure 1 shows a detailed cross section of the TITAN-I FPC including the manifolds, inlet and outlet headers, coolant channels, and the coolant flow directions. The first wall is a bank of circular coolant tubes. To adjust for the shorter toroidal length on the inboard side, the first-wall tubes slightly overlap on the inboard side of the torus. Therefore, two sets of coolant tubes are used with one set having a slightly larger poloidal diameter. The inside diameter and wall thickness of the first-wall coolant tubes are, respectively, 8 and 1.25 mm. The inside diameter of the first-wall tubes reflects a compromise between the total number of coolant tubes and the heat-transfer coefficient; reducing the diameter increases the heat-transfer coefficient, but it also increases the number of tubes and may reduce reliability (more likelihood of tube failure). The wall thickness of 1.25 mm includes a very conservative 0.25-mm allowance for erosion by various mechanisms. Sputtering erosion of the first wall by plasma particles is estimated to be negligible [1].

The overall thickness of the blanket and shield is 75 cm. The IBC zone is 28-cm wide, is located 1 cm behind the first wall, and consists of 6 rows of tubular coolant channels. Each coolant channel has an inside diameter of 4.75 cm and a wall thickness of 2.5 mm. The primary reason for using tubular coolant channels for the IBC zone, which results in more voids, is to reduce the number of load-bearing welded joints near the plasma (first wall). The resulting IBC zone consists of 18% structure, 72% lithium, and 10% void by volume.

The hot shield is located 1 cm behind the IBC, is 45-cm thick, and has two zones. The first zone is 30-cm thick and consists of 5 rows of square coolant channels with outer dimensions of 6 cm and a wall thickness of 5 mm. The inside corners are rounded and have the radius-to-wall thickness ratio of unity. The structure volume fraction is 30%, the coolant volume fraction is 70%, and there is no void. The second zone of the hot

Fig. 1. Elevation view of the TITAN-I first-wall and blanket coolant channels showing the manifolds, headers, and coolant flow direction.

shield is 15-cm thick and consists of 4 rows of rectangular channels with thick walls to increase the structure volume fraction in this zone. The structure volume fraction is 90% and the coolant volume fraction is 10%. The channels have outer dimensions of 11.25 cm by 3.75 cm and a wall thickness of 16.25 mm. The coolant flow in both the first wall and blanket are single pass in the poloidal direction. In the hot shield however, the poloidal flow circuit is double pass; lithium flows in through the first three square channels of the hot shield, makes a 180° turn at the inboard side, and exits through the last two square channels and the rectangular channels.

Thermal analyses for the first wall and blanket/shield are presented in Section 2. Analytical and semi-empirical analyses for pressure drop and material stress are dealt with in Section 3. These two sections provide equations for the thermal-hydraulic design code. The results of design analysis by this code are presented in Section 4. In Section 5, results of more accurate finite element analysis of material stress are given. Finally, Section 6 contains a summary and conclusions.

2. Thermal analyses for the first wall, blanket, and shield

The primary objective of thermal analysis is to accurately predict the wall temperature of the coolant channels, and thus allow a reasonable estimate of their lifetime. Figure 2 shows the size and heat load on a first-wall coolant tube. The heat load consists of radiation heat flux, q_0'', and volumetric nuclear heating in the wall, q_w''', and in the coolant, q_f'''. The radiation heat flux on the plasma-facing surface of a first-wall coolant tube is represented by a cosine distribution, with the maximum at $\theta = 0$, denoted as the point A in the figure.

The heat load is nearly constant along the axis of the tube. However, the surface heat flux varies circumferentially (along θ). The wall temperature can, therefore, be expressed as

$$T_w(\theta, z) = T_f(z) + \Delta T_f(\theta) + \Delta T_w(\theta), \tag{1}$$

where T_w is the wall temperature, ΔT_f is the film temperature drop, and ΔT_w is the temperature drop across the wall. The coolant temperature at a point z along the tube axis, $T_f(z)$, can be calculated from energy balance, and is given by

$$T_f(z) = T_{in} + \frac{(2/\pi)bq_0'' + a^2 q_f''' + (b^2 - a^2)q_s'''}{a^2 U \rho_f c_p} z, \tag{2}$$

where T_{in} is the inlet temperature of the coolant, L is tube length, U is the mean coolant velocity, and ρ_f and c_p, are, respectively, the density and specific heat capacity of the coolant. The first wall tube inner and outer radii are a and b, respectively.

One of the main constraints on the thermal-hydraulic design is the maximum temperature of the structure. Since the heat load is nearly constant axially, the maximum wall temperature, $T_{w,Max}$, occurs at the coolant exit point

$$T_{w,Max} = T_{ex} + (\Delta T_f + \Delta T_w)_{Max}, \tag{3}$$

where T_{ex} is the coolant exit temperature, $T_{ex} = T_f(z = L)$, and L is the length of the tube.

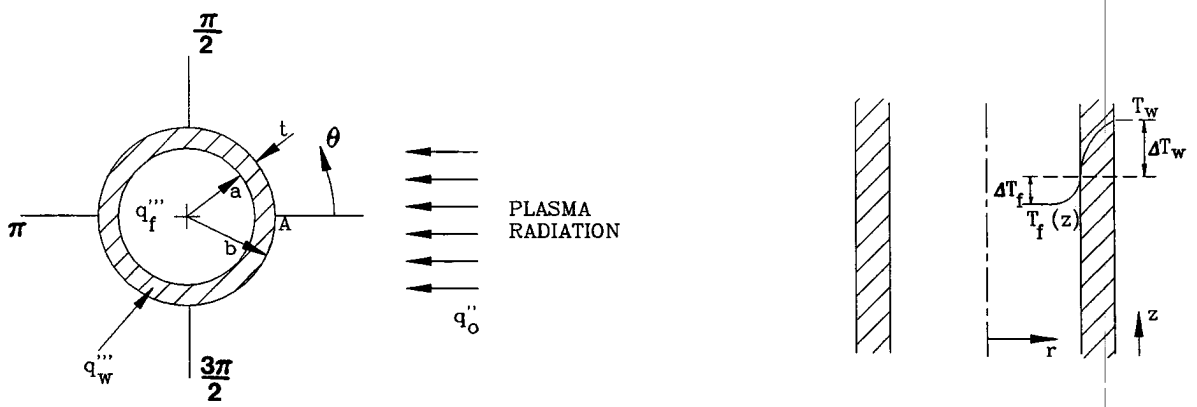

Fig. 2. The thermal-analysis model of the first-wall coolant tubes.

A 2-D numerical solution of the temperature field in the tube wall and coolant will give the value of the second term on the right-hand side of the eq. (3). However, a time-consuming numerical solution is not practical for a parametric design analysis. Since the tube wall is thin, heat conduction can be assumed to be in the radial direction only, thus decoupling the wall conduction from the convection in the coolant. Subsequent numerical solution has corroborated this assumption. Therefore, the temperature profile in the tube wall can be approximated by

$$T(r,\theta) = T_{wi}(\theta) + \frac{q'''_w b^2}{2k_w}\ln\left(\frac{r}{a}\right) - \frac{q'''_w}{4k_w}(r^2 - a^2) + \frac{q''_0 \cos(\theta) b}{k_w}\ln\left(\frac{r}{a}\right), \quad (4)$$

where T_{wi} is the temperature at the inner surface of the wall and k_w is the thermal conductivity of the wall material. The maximum wall temperature drop occurs at $\theta = 0$ (point A in Fig. 2), where the heat flux is maximum.

$$\Delta T_{w,Max} = \frac{q'''_w b^2}{2k_w}\ln\left(\frac{b}{a}\right) - \frac{q'''_w}{4k_w}(b^2 - a^2) + \frac{q''_0 b}{k_w}\ln\left(\frac{b}{a}\right). \quad (5)$$

The film temperature drop is calculated from the Nusselt number (Nu). A nonuniform surface heat flux strongly affects convective heat transfer and leads to circumferentially varying Nu [9–11]. Therefore, a 2-D analysis of the coolant temperature distribution has been performed for laminar flow. For the turbulent flow, an empirical correlation for Nu, corrected for the effect of nonuniformity of surface heat flux, is used. These are presented in the next two sections.

Thermal analyses of the blanket and shield are simpler than for the first wall. There is no radiation heat flux and the volumetric heating rates in individual coolant channels can be taken as uniform because the gradient of the volumetric heating across each channel is small. Therefore, the surface heat flux incident on the coolant is uniform, and the Nu is constant and known.

Figure 3 shows the cross section of a square coolant channel in the hot shield and the heat loads on it. From the desired coolant inlet and exit temperatures, the average coolant velocity is obtained by energy balance.

$$U = \frac{(b^2 - a^2)q'''_w + a^2 q'''_f}{a^2 \rho_f c_p (T_{ex} - T_{in})} L, \quad (6)$$

where $b = a + t$ and L is the length of the channel. The maximum wall temperature, as for the first wall, occurs at the exit point of the coolant.

$$T_{w,Max} = T_{ex} + \Delta F_f + \Delta T_w. \quad (7)$$

The film temperature drop is given by

$$\Delta T_f = \frac{(b^2 - a^2)q'''_w}{\mathrm{Nu}\, k_f}. \quad (8)$$

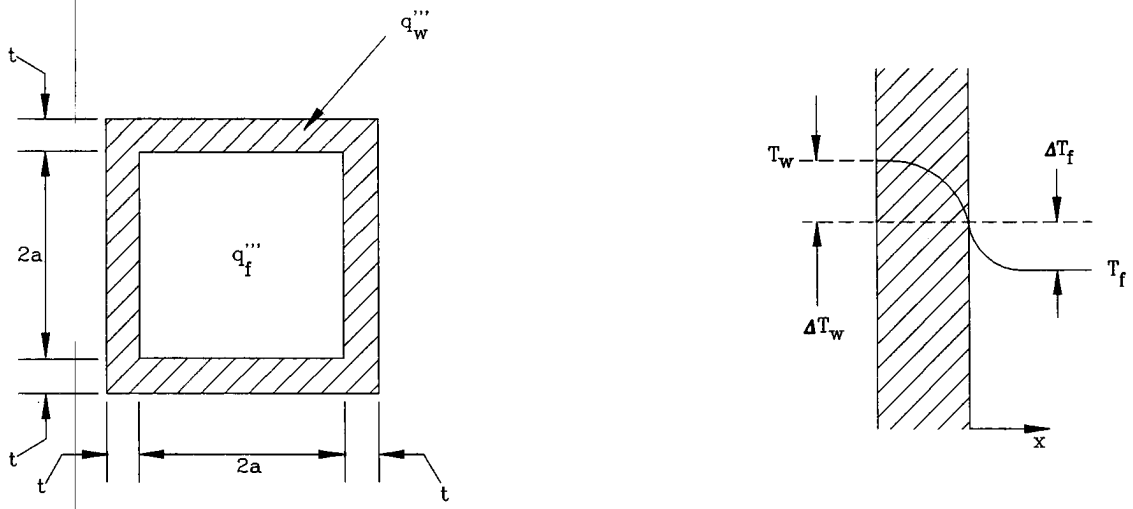

Fig. 3. The thermal-analysis model of the hot-shield coolant channels.

Similar expressions for U and ΔT_f can be written for rectangular shield channels. The flow is always laminar in the blanket and shield channels, and the Nu for laminar flow in a square channel with constant heat flux is 3.6 in the absence of the magnetic field. In the presence of the magnetic field with perpendicular Hartmann number (Ha) greater than 100, the average Nu is about 5.5.

The wall temperature drop can be estimated from a 1-D heat conduction in the wall. The temperature profile is parabolic, and the wall temperature drop can be approximated by

$$\Delta T_w = \frac{(b-a)^2 \theta_w'''}{2k_w}. \tag{9}$$

At the corners, ΔT_w will be slightly higher than that given by eq. (9), but the difference is not significant for thin walls.

2.1. Laminar heat transfer in the first-wall tubes

For a laminar coolant flow in the first-wall tubes, the film temperature drop is calculated from the 2-D solution of the convection equation

$$\frac{\partial^2 T}{\partial r^2} + \frac{1}{r}\frac{\partial T}{\partial r} + \frac{1}{r^2}\frac{\partial^2 T}{\partial \theta^2} = \frac{u(r)}{\alpha}\frac{\mathrm{d}T}{\mathrm{d}z}, \tag{10}$$

where $\alpha = k_f/(\rho_f c_p)$ is the thermal diffusivity of the coolant and $u(r)$ is the fully developed, laminar velocity profile of the coolant. To account for the flattening of the velocity profile caused by a perpendicular magnetic field, a power velocity profile for $u(r)$ is assumed

$$u(r) = U\left(\frac{m+2}{m}\right)\left[1 - \left(\frac{r}{a}\right)^m\right], \tag{11}$$

where U is the mean coolant velocity

$$U = \frac{2}{a^2}\int_0^a r u(r)\,\mathrm{d}r. \tag{12}$$

The exponent m would be large for a flat velocity profile, and $m = 2$ for a parabolic profile.

The boundary and symmetry conditions for eq. (10) are

$$k_f \left.\frac{\partial T}{\partial r}\right|_{r=a} = q''(\theta),$$
$$\left.\frac{\partial T}{\partial q}\right|_{\theta=0} = \left.\frac{\theta T}{\partial \theta}\right|_{\theta=\pi} = 0 \tag{13}$$

and the surface heat flux, $q''(\theta)$, is given by

$$q''(\theta) = \begin{cases} q''_{NH} + q''_0(\theta) & 3\pi/2 \le \theta \le \pi/2, \\ q''_{NH} & \pi/2 \le \theta \le 3\pi/2, \end{cases} \tag{14}$$

where q''_{NH} is the average heat flux at the interface between the tube wall and the coolant arising from the volumetric nuclear heat generation in the tube wall.

$$q''_{NH} = \frac{(b^2 - a^2)q'''_w}{2a}. \tag{15}$$

Equation (10) can be solved by the method of separation of variables [9,11], and the film temperature drop, ΔT_f, is found to be

$$\Delta T_f(\theta) = f(m)\frac{a}{\pi k_f}\int_0^{2\pi} q''(\omega)\,\mathrm{d}\omega - \frac{a}{\pi k_f}\int_0^{2\pi} q''(\omega)\ln\left[2\sin\left(\frac{\theta-\omega}{2}\right)\right]\mathrm{d}\omega, \tag{16}$$

where

$$f(m) = \frac{(m+2)^2 - 4}{4m(m+2)} - \frac{(m+2)^2}{m^2} \times \left[\frac{m}{8(m+4)} - \frac{m+2}{(m+1)(m+2)^3}\right]. \tag{17}$$

Using eq. (16), the Nusselt number, Nu(θ), can be determined.

$$\mathrm{Nu}(\theta) = \frac{2aq''(\theta)}{k_f \Delta T_f(\theta)}. \tag{18}$$

Equation (18) shows that the Nu varies along the circumference of the tube. For a parabolic velocity profile ($m = 2$) and a uniform heat flux, the eqs. (16) and (18) give Nu = 48/11 = 4.36. When the velocity profile is flat ($m \to \infty$) and the heat flux is uniform, Nu = 8. These are the well-known values of Nu for laminar parabolic and slug flows in a circular pipe.

When the surface heat flux is not uniform, the Nu and film temperature drop vary along the circumference of the tube. Figure 4 shows this variation, as computed from the eqs. (16) and (18) for the case of $q''_0 = 4.6$ MW/m^2 and $q''_{NH} = 0.12$ MW/m^2. The Nu is positive for θ from 0° to about 90°. At a point in the vicinity of $\theta = 90°$, the Nu is infinite, reflecting that ΔT_f is zero at this point. Beyond this point, Nu becomes negative, because the average coolant temperature is higher than the surface temperature.

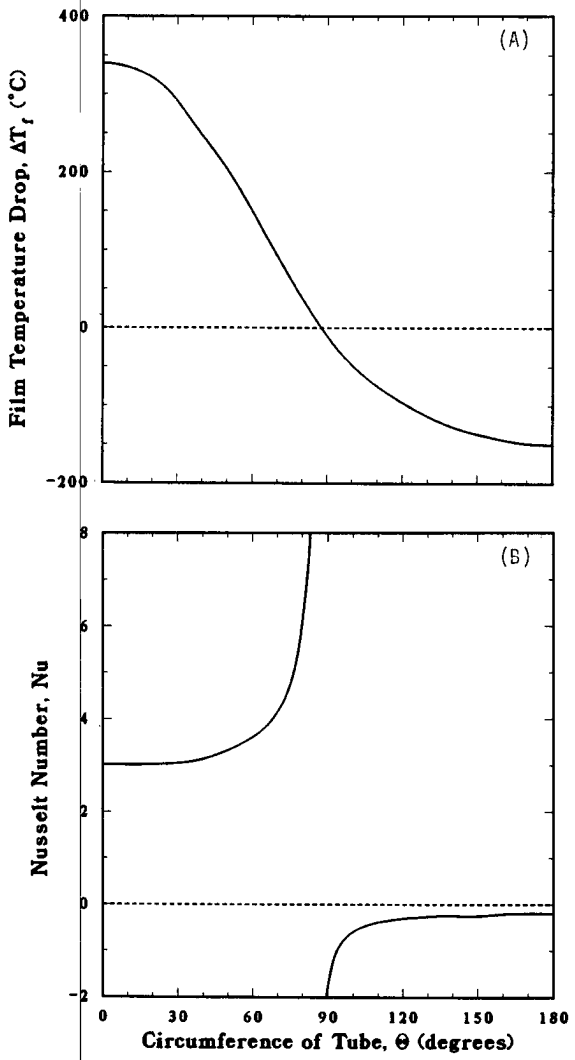

Fig. 4. Variation of the Nusselt number (A) and the film temperature drop (B) around the circumference of the coolant tube for $q_0'' = 4.6$ MW/m^2 and $q_{NH}'' = 0.12$ MW/m^2.

The maximum film temperature drop occurs at $\theta = 0$ (point A in Fig. 2), where $Nu \simeq 3.0$ instead of the average value of 7.1, as has been calculated for uniform heat flux and transverse Ha greater than 100 [12]. This lower value of the Nu number should be used in determining the film temperature drop; otherwise the maximum wall temperature will be seriously underestimated.

The effect of nonuniform surface heat flux can be reduced or eliminated by utilizing the swirl flow produced, for example, by helical vanes fitted inside the tube [13]. The curvature of the tube also introduces secondary flow patterns similar to swirl flow [14]. However, the effect of the magnetic field on the swirl flow has not been investigated and, therefore, the swirl-flow patterns have not been used for the TITAN-I design.

2.2. Turbulent heat transfer in the first-wall tubes

The Nu in turbulent flow can be substantially higher than in laminar flow. The use of turbulent flow can increase the design heat flux on the first wall. However, a magnetic field tends to suppress turbulence in the flow of an electrically conducting fluid, and the onset of turbulence takes place at higher Reynolds numbers (Re) (for non-MHD pipe flow, the transition Re is 2300). The Re is defined as $Re = \rho_f U d_h / \eta_f$, where d_h is the hydraulic diameter of the channel and η_f is the viscosity of the coolant.

Experimental data on MHD turbulent flow are limited. Some experimental data in the presence of a transverse magnetic field are reported [15–17] with Ha ranging up to 1300. The Ha is defined as $Ha = Bd_h\sqrt{\sigma_f/\eta_f}$, where B is magnetic field strength and σ_f is the electrical conductivity of the coolant. Experimental data in the presence of longitudinal magnetic field are also reported [18,19], but the Ha was low (up to about 150). The onset of turbulence was detected from pressure fluctuations and skin friction data, and it has been shown that the onset of turbulence is delayed by both the transverse and longitudinal fields, the effect of the transverse field being stronger. The transition Reynolds number, Re_t, corresponding to the onset of the turbulence, has been proposed to be directly proportional to the Ha as [20]

$$Re_t \geq \begin{cases} C_1 Ha_\perp & \text{for perpendicular field,} \\ C_2 Ha_\parallel & \text{for parallel field,} \end{cases} \tag{19}$$

where $Ha_\perp$ and $Ha_\parallel$ are, respectively, the transverse and longitudinal Hartmann numbers and C_1 and C_2 are constants. Hoffman [20] suggested $C_1 = 500$ and $C_2 = 60$. The data from Gardner and Lykoudis [15], which extends to $Ha_\perp = 1300$, suggest $C_1 \leq 250$, while the data from Globe [18] suggest $C_2 \simeq 40$. Lykoudis [21] suggested a value of 236 for C_1 while Branover et al. [22] suggested a value of 155 for circular tubes and square ducts.

An interesting aspect of Equation 19 is that the turbulent velocity, v_t, is independent of the channel size, and is solely determined by the magnetic field strength and the coolant properties

$$v_t \geq \begin{cases} C_1 B_\perp \left(\sqrt{\sigma_f \eta_f}/\rho_f\right), \\ C_2 B_\parallel \left(\sqrt{\sigma_f \eta_f}/\rho_f\right), \end{cases} \tag{20}$$

where $B_\perp$ and $B_\parallel$ are, respectively, the perpendicular and parallel magnetic fields. Using the conservative values of $C_1 = 500$ and $C_2 = 60$ [20], a minimum lithium flow velocity of 20 m/s is estimated for MHD turbulent flow in the TITAN-I first-wall tube. The longitudinal (poloidal) magnetic field is the dominant field here.

Few studies are available on the turbulent-flow heat transfer in liquid metals in the presence of a magnetic field. Kovner et al. [23] performed experiments on the effect of a longitudinal magnetic field on turbulent heat transfer in liquid-galium flow in a tube. The following empirical correlation for Nu was then proposed

$$\mathrm{Nu} = 6.5 + \frac{0.005\mathrm{Pe}}{1 + 1890(\mathrm{Ha}_\parallel/\mathrm{Re})^{1.7}}, \qquad (21)$$

where $\mathrm{Pe} = \mathrm{RePr}$ is the Peclét number and $\mathrm{Pr} = \eta_f c_p/k_f$ is the Prandtl number. Equation (21) reduces to that for ordinary turbulent flow for $\mathrm{Ha}_\parallel = 0$. This equation also predicts the expected effects of the magnetic field: the Nu increases with increasing field strength, while for a given Re, the Nu approaches the value for laminar flow as $\mathrm{Ha}_\parallel$ increases. Conversely, for a given $\mathrm{Ha}_\parallel$, the Nu approaches its value for standard liquid-metal correlations without magnetic field as Re is increased. Equation (21) is based on experimental data up to $\mathrm{Ha}_\parallel = 550$. Since it predicts the limiting values of Nu correctly, it is assumed to hold beyond the correlation range of $\mathrm{Ha}_\parallel$. Further experiments are necessary to corroborate this assumption.

The experimental data from Gardner and Lykoudis [24], with transverse magnetic field and $\mathrm{Ha}_\perp$ ranging up to 1300, show similar dependence. Krasilnikov [25] performed a numerical study on turbulent-flow heat transfer in a channel between two parallel plates in the presence of a transverse magnetic field. His results also show similar effects of the magnetic field on turbulent-flow heat transfer. Branover et al. [22] reported experimental evidence to suggest that, under certain conditions, the magnetic field may increase turbulence intensity in an anisotropic fashion and, as a result, the total thermal diffusivity will be greatly increased.

For the TITAN-I design, eq. (21) is used. Figure 5 shows the variation of Nu with Pe for $B = 0$, $\mathrm{Ha}_\parallel = 1000$, and $\mathrm{Ha}_\parallel = 3040$ (for TITAN-I first wall). The range of the experimental data is also shown. It is seen that the flow remains laminar up to large values of Pe as the Ha is increased.

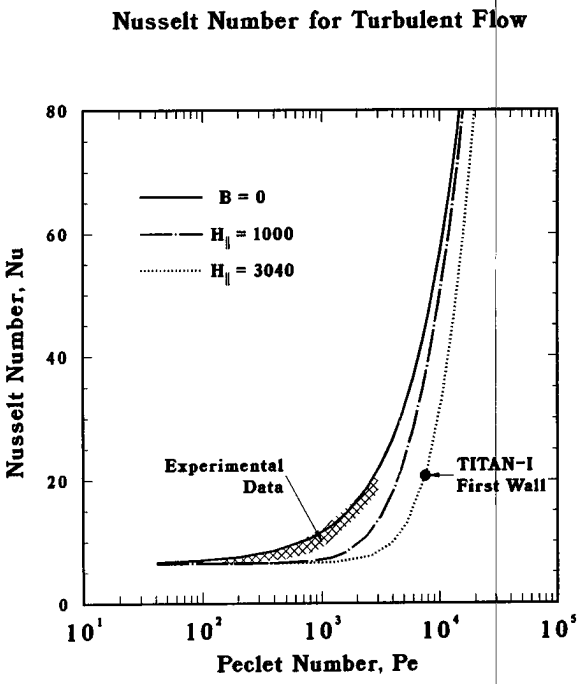

Fig. 5. Variation of the Nusselt number, Nu, with the Peclét number, Pe, for turbulent flow as predicted by eq. (21). The range of experimental data as well as the operating point of the TITAN-I first wall are also shown. The Nu from this graph is reduced by a factor of 2 to account for the nonuniformity of heat flux on the TITAN-I first wall.

The nonuniform circumferential heat flux on the first-wall tubes will reduce the turbulent Nu at the point of highest heat flux, as has been shown before for the case of laminar flow (Section 2.1). Until further data become available, Nu given by eq. (21) is reduced by a factor of 2 for the TITAN-I design to account for this nonuniform circumferential heat flux.

3. Pressure drop and material stress

A liquid metal flowing in the presence of a perpendicular magnetic field encounters a combination of pressure drops caused by the magnetic body force and friction,

$$\Delta p = \Delta p_f + \Delta p_{\mathrm{MHD}}. \qquad (22)$$

In a straight channel, the friction pressure drop, Δp_f, is given by

$$\Delta p_f = f\frac{\rho_f U^2 L}{2d_h}, \tag{23}$$

where U is the mean flow velocity of the coolant, L is the length of the channel, ρ_f is the density of the liquid metal, and d_h is the hydraulic diameter of the channel. The parameter f is the friction factor: for laminar flow, $f = 64/\mathrm{Re}$; for turbulent flow, f is given as a function of Re and the surface roughness in the Moody friction-factor chart [26]. Semi-empirical equations are also available for friction pressure drop at bends, contractions, and expansions.

For a uniform straight channel in the presence of a constant, transverse magnetic field ($B_\perp$), the associated MHD pressure drop is given by [27]

$$\Delta p_{MHD} = \sigma_f U B_\perp^2 a\frac{\phi}{1+\phi}L. \tag{24}$$

For a rectangular channel, a is half the length of the inner side of the channel parallel to the magnetic field; for a circular tube, a is the inside radius. The wall-to-coolant electrical-conductance ratio, ϕ, is

$$\phi = \frac{\sigma_w t}{a\sigma_f}, \tag{25}$$

where t is the channel wall thickness and σ_w and σ_f are, respectively, the electrical conductivities of the wall material and the coolant.

It is difficult to derive analytical relationships for the MHD pressure drops in a bend, a contraction, or a channel with a varying cross section or in a varying magnetic field. Semi-empirical equations are, however, available for these cases. The MHD pressure-drop equations which appear to be best suited for the TITAN-I design are discussed below [3]. At a contraction or along the length of a channel, where the magnetic field is varying, the MHD pressure drop is estimated by the following equation.

$$\Delta p = 0.2\sigma_f U B_\perp^2 a\sqrt{\phi}\,. \tag{26}$$

For flow through a bend, if both legs of the bend are normal to the magnetic field, the MHD pressure drop is zero. If one leg of the bend is normal and the other leg is parallel, the MHD pressure drop is predicted by

$$\Delta p = \sigma_f U B_\perp^2 a\sqrt{\phi}\,. \tag{27}$$

In order to complete the thermal-hydraulic design, pressure and thermal stresses in the coolant channels were estimated by 1-D axisymmetric equations for a thick-walled tube [28,29]. The radial pressure stress, the hoop stress, and the equivalent pressure stress are given, respectively, by

$$\sigma_r^p(r) = \frac{a^2 p_i}{b^2-a^2}\left(1-\frac{b^2}{r^2}\right),$$

$$\sigma_\theta^p(r) = \frac{a^2 p_i}{b^2-a^2}\left(1+\frac{b^2}{r^2}\right),$$

$$\sigma_{eq}^p(r) = \sqrt{\tfrac{1}{2}\left[\left(\sigma_r^p-\sigma_\theta^p\right)^2+\left(\sigma_r^p\right)^2+\left(\sigma_\theta^p\right)^2\right]}\,, \tag{28}$$

where p_i is the coolant pressure, and the pressure outside the tube is assumed zero. The radial, circumferential, and equivalent thermal stresses are given, respectively, by

$$\sigma_r^T(r) = \frac{\alpha E}{r^2}\left[\frac{r^2-a^2}{b^2-a^2}\int_a^b rT(r)\,\mathrm{d}r - \int_a^r rT(r)\,\mathrm{d}r\right],$$

$$\sigma_\theta^T(r) = \frac{\alpha E}{r^2}\left[\frac{r^2+a^2}{b^2-a^2}\int_a^b rT(r)\,\mathrm{d}r + \int_a^r rT(r)\,\mathrm{d}r - r^2T(r)\right],$$

$$\sigma_{eq}^T(r) = \sqrt{\tfrac{1}{2}\left[\left(\sigma_r^T-\sigma_\theta^T\right)^2+\left(\sigma_r^T\right)^2+\left(\sigma_\theta^T\right)^2\right]}\,, \tag{29}$$

where α is the coefficient of linear expansion and E is the Young's modulus of the tube material. Equation (4), with $\theta = 0$, is used for the temperature profile in the above equations.

For rectangular coolant channels of the shield, the thermal stress is estimated by

$$\sigma^T \simeq \frac{\alpha E \Delta T_w}{2(1-\nu)}, \tag{30}$$

where ν is the Poisson ratio of the wall material. It is more difficult to estimate the pressure stress in square or rectangular channels because of bending and corner effects. A very rough estimate can be obtained from

$$\sigma^p \simeq \frac{a}{t}p_i. \tag{31}$$

The effect of bends and corners depends on the ratio of the side length to the wall thickness, a/t and on the corner fillet radius. A 2-D analysis of the pressure stress in square channels was performed by using the

finite-element code, ANSYS, and the results are reported in Section 5. The maximum stress in the coolant channel wall in the shield is obtained as a function of a/t. For the parametric survey of the thermal-hydraulic design window, the size of each square or rectangular coolant channel is chosen such that for a given coolant pressure, the ratio a/t is smaller than the maximum value that is predicted by finite-element analysis.

4. Thermal-hydraulic design window

The first wall intercepts a radiation heat flux of 4.6 MW/m^2. In order to remove such a high heat flux, the first wall is designed to be of small-diameter, circular tubes. Other thermal-hydraulic design features of TITAN-I are the separation of the first-wall and blanket coolant circuits and the use of MHD turbulent-flow heat transfer to remove the high surface heat flux at the first wall. Figure 6 is a flowchart of the computer code developed to perform the design calculations [30].

The objective of design calculations is to obtain a thermal-hydraulic design window for selecting a design point. The primary interest is to realize as high a coolant exit temperature as possible for a given radiation heat flux on the first wall. The constraints are the design limits on the maximum allowable structure temperature, material stress, and pumping power. The coolant exit temperature varies directly with the wall temperature limit and inversely with the pumping power and stress limits. Other parameters influencing the design window are the neutron wall loading, the coolant channel size, and the coolant inlet temperature. Changing any of these parameters would alter the design window. Relevant parameters for the thermal-hydraulic design are given in Table 2.

The input to the code includes the reactor parameters, physical properties of the coolant and structural material, coolant-channel geometry, and design constraints. For a given first-wall tube size and a given radiation heat flux on the first wall, the maximum wall temperature drop for the first-wall tube is found from eq. (5). Assuming a laminar flow, the maximum film temperature drop is then calculated from eq. (16), and the maximum permissible coolant exit temperature for the first wall, $T_{ex,FW}$, is obtained from eq. (3). With this exit temperature, the average coolant velocity is computed from eq. (2). If $T_{ex,FW} \leq T_{in}$, or the coolant velocity is greater than or equal to the turbulent velocity, no solution for the laminar flow exists. In this case, the coolant velocity is set equal to the turbulent veloc-

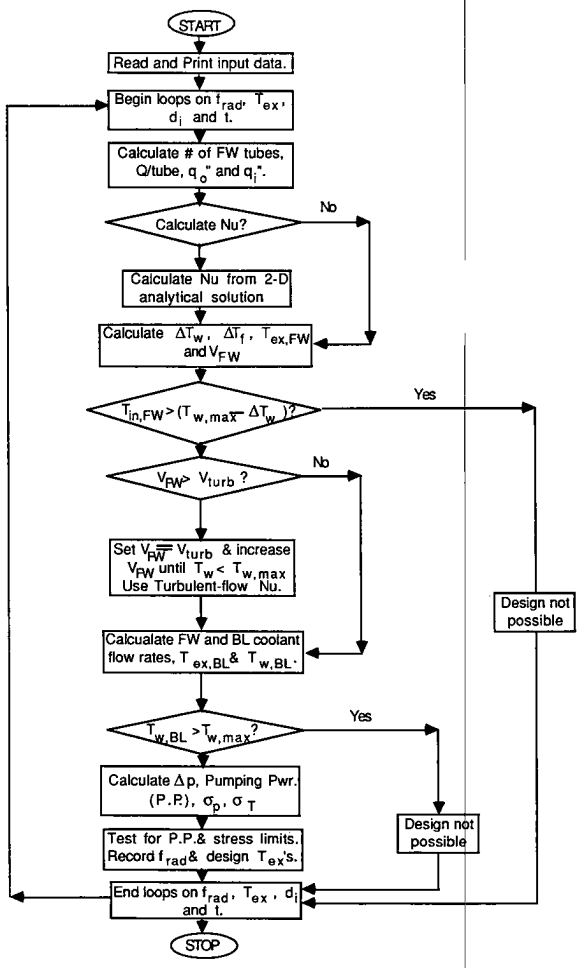

Fig. 6. Flowchart of the TITAN-I thermal-hydraulic design code [30].

Table 2
Thermal-hydraulic design parameters

Major radius	3.9 m
First wall radius	0.66 m
Total thermal power	2918 MW
Structural material	V-3Ti-1Si
Primary coolant	lithium
First-wall heat flux	4.6 MW/m^2
Poloidal field at first wall	5.4 T
Toroidal field at first wall	−0.36 T
Coolant inlet temperature	320°C
Structure temperature limit	750°C
Pressure stress limit	108 MPa
Thermal stress limit	300 MPa
Pumping power limit [a]	50 MW

[a] Pumping-power limit is set at 5% of the net electric output.

ity, and the film temperature drop, ΔT_f, is recalculated using the Nu for turbulent flow from eq. (21) (which is halved to account for nonuniform circumferential heat flux). The coolant exit temperature is found using this value of the film temperature drop in the turbulent regime and, if necessary, the coolant velocity is increased until the maximum structure temperature, $T_{w,Max}$, is within the design limit.

For design window calculations, the blanket is treated as a lumped-parameter system. The blanket coolant exit temperature, $T_{ex,BL}$, is determined by energy balance so that, using the determined $T_{ex,FW}$, the mixed temperature of the first-wall and blanket circuits would match the input value of average coolant exit temperature. The film and wall temperature drops are calculated from eqs. (8) and (9), and the maximum temperature of the blanket-coolant channel is found from eq. (7). If the maximum wall temperature is within the design limit, the calculated average coolant exit temperature is recorded as the highest possible exit temperature for the current radiation heat flux and structure temperature limit.

Pressure drop and pumping power are calculated from the coolant velocity. The equations given in Section 3 are used to estimate the MHD and friction pressure drops. The coolant pressure is highest at the inlet of a coolant channel. Pressure stresses are, therefore, determined at the inlet point of all circuits.

The above procedures are repeated for different values of mixed coolant exit temperature and then for a range of heat fluxes on the first wall.

Figure 7 illustrates the thermal-hydraulic design window for the TITAN-I FPC and shows that a design with a radiation heat flux on the first wall of 4.9 MW/m^2 is possible. The sudden change in the slope of the top curve in Fig. 7, corresponding to the structure temperature limit, is caused by the change in flow from laminar to turbulent. Also, the pumping-power limit of 5% of electric output is more restrictive in this range of heat flux than the pressure stress of 108 MPa. The thermal stress limit is not reached up to the maximum heat flux on the first wall.

The coolant flow paths in the first-wall and blanket circuits of TITAN-I are shown in Fig. 8, and the variation of the coolant pressure along the length of the coolant channels of the first wall and blanket is shown in Fig. 9. For the blanket components, the pressure distributions in rows 1 and 6 of the coolant channels of the IBC zone are shown. The pressure drop in the hot shield is negligible because of low coolant flow velocity and zero perpendicular (toroidal) magnetic field; the hot shield lies beyond the IBC blanket.

The coolant flow velocity in the TITAN-I first-wall tube is 21 m/s and the maximum pressure drop is 10 MPa. Since substantial simplification is made by cooling two components (first wall and divertor) from the same cooling circuit, the delivery pressure of the coolant pump for the first-wall and divertor coolant circuits is set at 12 MPa, the maximum pressure drop in the divertor coolant circuit [1]. The coolant pressure for the first wall is then reduced to 10 MPa by using an orifice.

The coolant velocities in rows 1 and 6 (last) of IBC coolant channels are, respectively, 0.5 and 0.2 m/s. The pressure drop is 3.0 MPa in row 1 and 0.5 MPa in row 6. The supply pressure of the blanket coolant pump is 3 MPa. Orifices are used to reduce the pressure to the required values at the inlet of each row of IBC channels.

The maximum equivalent pressure and thermal stresses are, respectively, less than 100 and 150 MPa, calculated from the analytical equations in the previous section. The pressure stress is evaluated at the end of life of the first wall when the wall thickness is reduced due to sputtering erosion. The allowable pressure stress is a function of material temperature, increasing with decreasing temperature. For a coolant tube, the pres-

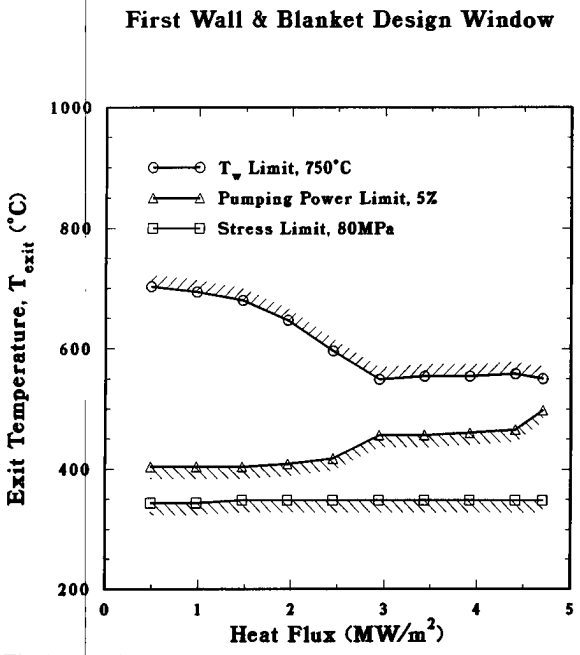

Fig. 7. The thermal-hydraulic design window for the TITAN-I FPC.

A – Entrance
AB– Straight Duct
– Varying B–Field
B – Inlet/Contraction
– Bend
BC– Straight Tube
C – Bend, Expansion
CD– Straight Duct
– Varying B–Field
D – Expansion

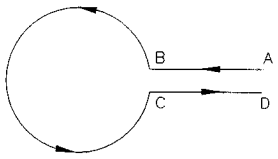

FW Flow Circuit

E – Entrance
EF– Straight Duct
– Varying B–Field
F – Inlet/Contraction
– Bend
FG– Straight Channel
G – Bend, Expansion
GH– Straight Duct
– Varying B–Field
H – Expansion

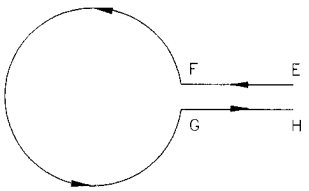

Blanket Channel Flow Circuit

Fig. 8. Schematic of the flow paths in the first-wall and blanket coolant channels.

sure is highest at the inlet and lowest at the exit. On the other hand, the wall temperature is lowest at the inlet and highest at the exit. Figure 10 presents the pressure stress, average wall temperature, and the allowable stress along the length of a first-wall tube. The pressure stress in the first-wall tubes is 4 to 6 times smaller than the allowable stress. The stresses in the blanket channels are well below the design limits because of the low pressure, thick channel walls, and the small temperature gradient. Finite-element analyses of the pressure and thermal stresses in the first-wall and blanket components have verified these results (Section 5).

The thermal power is converted into electricity by two Rankine steam cycles to take advantage of the much higher exit temperature of the blanket/shield coolant (700°C compared with 442°C for the first wall coolant). The thermal powers from the first wall and blanket/shield are converted at 37% and 46.5% efficiencies, respectively [1,31]. This gives an overall gross efficiency for TITAN-I of 44%. The power cycle analysis was performed by the code PRESTO [32]. The main results of the thermal-hydraulic analyses of the TITAN-I FPC are given in Tables 3 through 5.

Two other noteworthy issues in this design are the circulation of the primary coolant and the erosion of the first wall. These are discussed briefly in the next two sections.

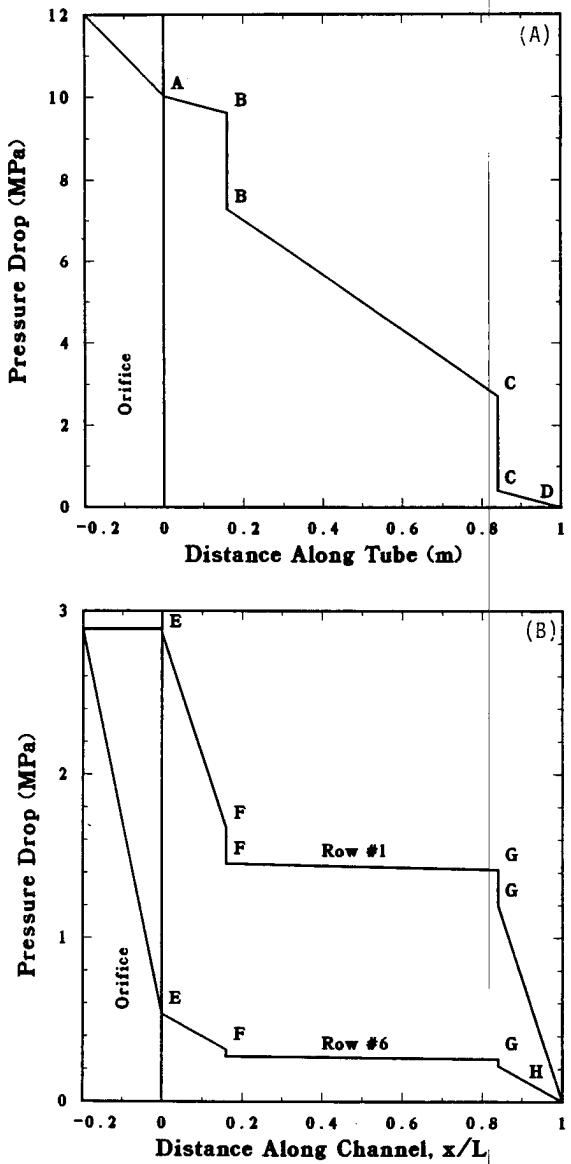

Fig. 9. Pressure distributions in the first-wall (A) and the blanket coolant channels (B). The pressure drop in the hot shield is negligible. Points A through H correspond to the coolant flow path in Fig. 8.

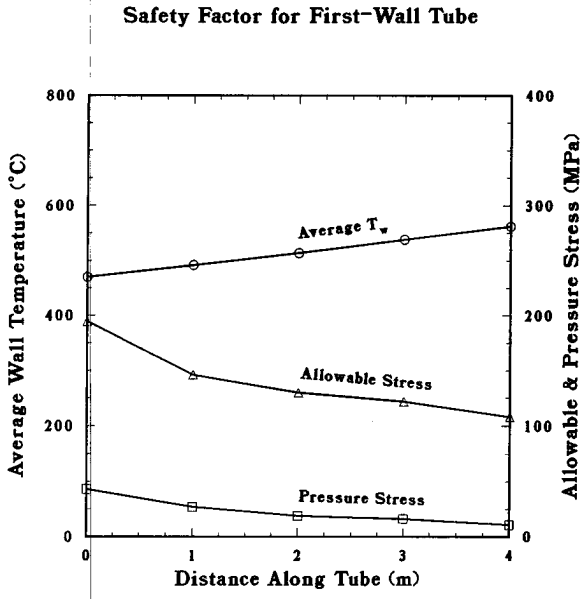

Fig. 10. Safety factors for pressure stress in the first-wall tube.

Table 3
Thermal-hydraulic design of TITAN-I first wall

Pipe outer diameter, b	10.5 mm
Pipe inner diameter, a	8.0 mm
Wall thickness, t	1.25 mm
Erosion allowance	0.25 mm
Structure volume fraction	0.400
Coolant volume fraction	0.375
Void volume fraction	0.225
Coolant inlet temperature, T_{in}	320°C
Coolant exit temperature, $T_{ex,FW}$	442°C
Maximum wall temperature, $T_{w,Max}$	747°C
Maximum primary stress	50 MPa
Maximum secondary stress	288 MPa
Coolant flow velocity, U	21.6 m/s
Pressure drop, Δp	10 MPa
Total pumping power [a]	37.7 MW
Reynolds number, Re	1.90×10^5
Magnetic Reynolds number, Re_m	0.48
Parallel Hartmann number, $H_\parallel$	3.04×10^3
Perpendicular Hartmann number, $H_\perp$	2.01×10^2
Parallel magnetic interaction parameter, $N_\parallel$	48.6
Perpendicular magnetic interaction parameter, $N_\perp$	0.21
Nusselt number, Nu [b]	10.35
Prandtl number, Pr	4.08×10^{-2}
Peclét number, Pe	7.76×10^3

[a] A pump efficiency of 90% is assumed.
[b] Turbulent flow, half the correlation value.

4.1. Coolant circulation

The pressure drops in the first-wall and divertor circuits are much higher than in the blanket circuit. The maximum pressure drops in the divertor, first-wall, and blanket-coolant circuits are, respectively, 12, 10, and 3 MPa. In order to simplify the design, the first-wall and divertor coolants are supplied from the same circuit. Therefore, two separate coolant pumps are used to circulate the lithium: one for the first-wall and divertor circuit, and the second for the blanket and shield circuit. The pressure drop in the intermediate heat exchanger is small (~ 0.1 MPa). The delivery pressure of the first-wall and divertor coolant pump is 12 MPa. A single orifice is used to reduce the lithium pressure to 10 MPa for the first-wall circuit (Fig. 9). Additional orifices are used, where necessary, to reduce the coolant pressure from 12 MPa to the required inlet pressures of the individual rows of divertor coolant tubes. The blanket coolant pump has a delivery pressure of 3 MPa. Orifices are used to reduce the pressure to match the requirement of each row of IBC and shield coolant channels.

Figure 11 is a schematic of the coolant flow in TITAN-I. All of the coolant circulation pumps are centrifugal pumps. The pump capacity, Q (gallon per

Table 4
Thermal-hydraulic design of TITAN-I IBC

Pipe outer diameter	52.5 mm
Pipe inner diameter	47.5 mm
Wall thickness	2.5 mm
Structure volume fraction	0.18
Coolant volume fraction	0.72
Void volume fraction	0.10
Coolant inlet temperature	320°C
Coolant exit temperature	700°C
Maximum wall temperature	747°C
Maximum primary stress [b]	30 MPa
Maximum secondary stress	5 MPa
Coolant velocity [b]	0.5 m/s
Pressure drop [b]	2.8 MPa
Total pumping power [a]	6.0 MW
Reynolds number [b]	2.75×10^4
Magnetic Reynolds number [b]	0.066
Parallel Hartmann number [b]	1.9×10^4
Perpendicular Hartmann number [b]	1.3×10^3
Parallel magnetic interaction parameter [b]	1.33×10^4
Perpendicular magnetic interaction parameter [b]	6.15×10^1
Nusselt number [b]	5.6

[a] A pump efficiency of 90% is assumed.
[b] Values for the first row of IBC tubes.

Table 5
Thermal-hydraulic design of TITAN-I hot shield

Coolant inlet temperature	320°C
Coolant exit temperature	700°C
Maximum wall temperature	747°C
Pressure drop	0.1 MPa
Total pumping power [a]	3.0 MW
First zone	
Channel outer dimensions	60×60 mm
Wall thickness	5 mm
Structure volume fraction	0.30
Coolant volume fraction	0.70
Reynolds number	9.79×10^3
Parallel Hartmann number [b]	7.00×10^3
Perpendicular Hartmann number [b]	nil
Nusselt number	3.6
Second zone	
Channel outer dimensions	112.5×37.5 mm
Wall thickness	16.25 mm
Structure volume fraction	0.90
Coolant volume fraction	0.10
Reynolds number	1.84×10^3
Parallel Hartmann number [b]	1.30×10^3
Perpendicular Hartmann number [b]	~0
Nusselt number	8.2

[a] A pump efficiency of 90% is assumed.
[b] Values for $B_p \sim 2T$, $B_t \sim 0$.

minute, GPM), the pump speed, N (rpm), and the head, H (feet of the fluid pumped) of a centrifugal pump are related through the specific speed, N_s (rpm) [33]. Conversion to SI units (Q in m^3/s and H in m) results in

$$N_s = 2.12\times10^{-2}\frac{N\sqrt{Q}}{H^{3/4}}. \quad (32)$$

The fusion power core of TITAN-I is divided into three sectors separated by the three divertor modules.

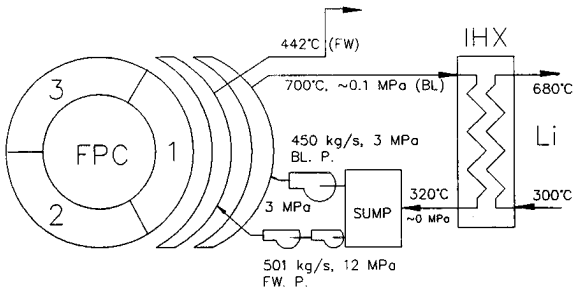

Fig. 11. A schematic of the coolant circulation in the TITAN-I reactor.

The coolant flow rates per sector are 1.2 m^3/s (16,000 GPM) in the first-wall and divertor circuit, and 1.1 m^3/s (14,500 GPM) in the blanket and shield circuit. Centrifugal pumps for feed water in large central stations have stage pressure of 7 MPa and speed of 9000 rpm [33]. Therefore, a two-stage centrifugal pump with stage pressure of 6 MPa is suggested for the first-wall/divertor circuit and a single-stage pump for the blanket/shield circuit. From eq. (32), the required speed of the first-wall and divertor pump, at the capacity of 1.2 m^3/s, is 8100 rpm. The required speed of the blanket and shield pump is 5200 rpm at the capacity of 1.1 m^3/s. The specific speed is assumed to be 2000 rpm, which results in a pump efficiency of about 90%, based on commercial pump data [33].

4.2. First-wall erosion

Material erosion is one of the critical issues of the first-wall design. While a thin wall will reduce both the temperature drop across the wall of the coolant tube and the thermal stress, a thicker wall is necessary to reduce the pressure stress and allow for material erosion. The erosion allowance should be such that enough material remains to keep the pressure stress within the design limit at the end of life of the first wall. The erosion allowance for the first-wall tube is 0.25 mm, which is assumed to be adequate according the present state of understanding of the erosion mechanisms and the quantification of various erosion rates. Several potential processes for the erosion of first-wall material have been identified:

(1) Sputtering by ions and neutral atoms,
(2) Erosion by the high-velocity coolant impact and/or cavitation,
(3) Mechanical abrasion caused by the impact of high-velocity suspended foreign particles,
(4) Fretting abrasion resulting from flow-induced vibration of the coolant tubes,
(5) Corrosion caused by chemical reaction with the coolant.

The TITAN-I reactor operates with a highly radiative plasma and utilizes high-recycling divertors as the impurity-control system. As a result, the particle flux on the first wall is substantially reduced and the edge-plasma temperature is below the sputtering threshold. The sputtering erosion of the TITAN-I first wall is expected to be less than 0.1 mm/y [1]. Erosion from the impact of lithium and foreign particles is expected to be very small. Cavitation is not likely because the pressure in the coolant channels is always higher than

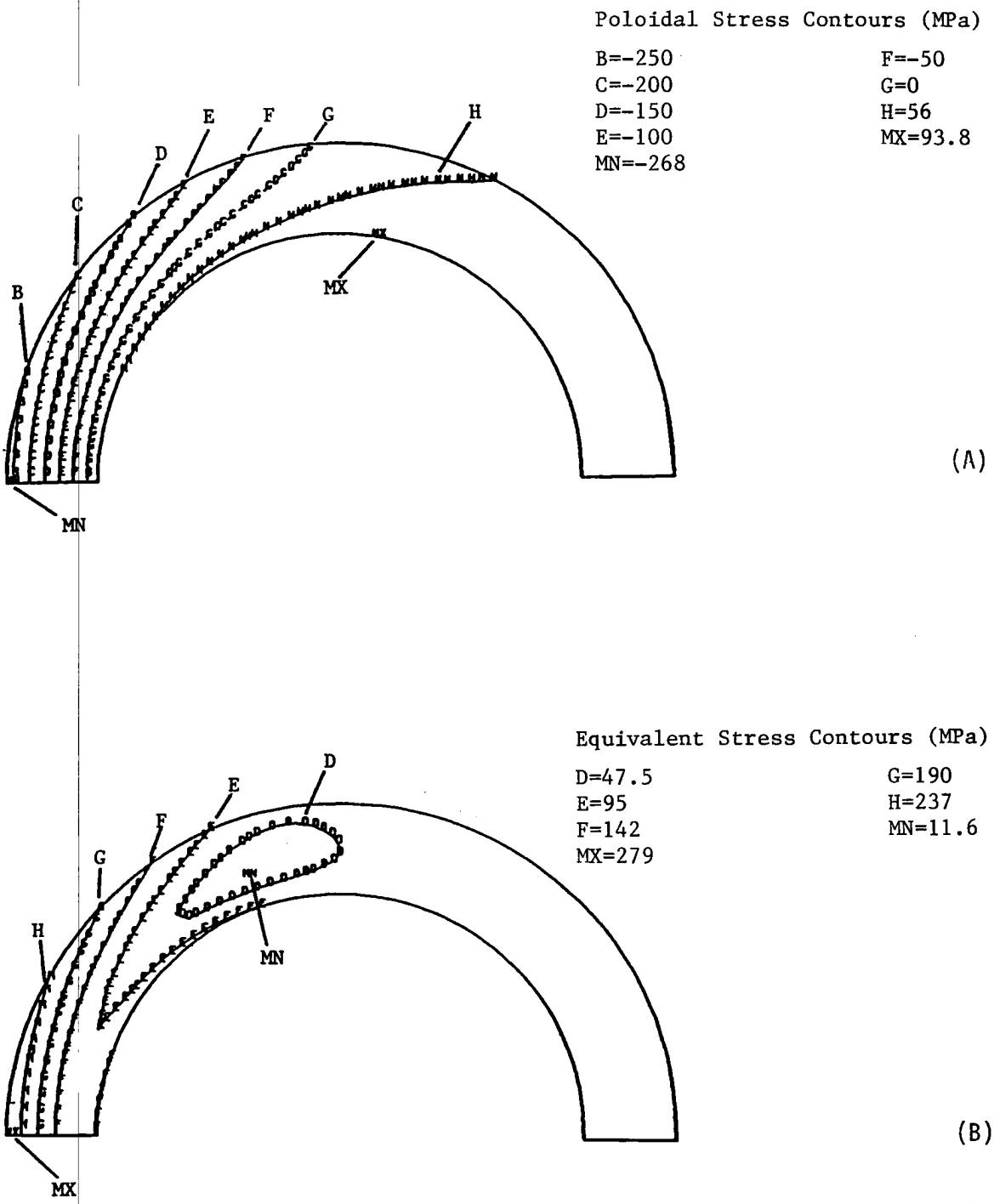

Fig. 12. Equivalent thermal stress in the first wall of the TITAN-I design from the plane-stress (A) and axisymmetric model (B).

the vapor pressure. To prevent vibration, the first-wall coolant tubes are rigidly attached to each other by tack-welding the adjacent tubes together at the back.

Corrosion of vanadium alloys by lithium is not well tested at this time. Hays [34] measured a total depth of material removal of 7.6×10^{-3} mm (or 0.133 mm/y) in a 500-h test of corrosion resistance of Nb–1Zr alloy exposed to 1073°C to 1143°C liquid lithium flowing at 50 m/s. Given the very low corrosion rate of Nb–1Zr by hot lithium flowing at 50 m/s, it is assumed that the lithium coolant at 350°C flowing in the first-wall tube at 21 m/s will have a very small corrosion effect on vanadium alloys.

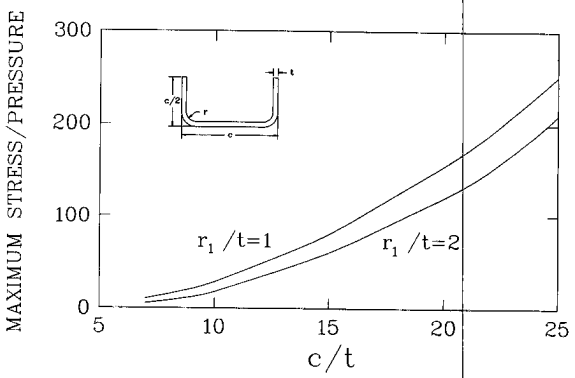

Fig. 13. Geometry of the shield channels and the sensitivity of the pressure stresses to the channel geometry.

5. Finite-element structural analysis

Two-dimensional thermal and stress analyses of the TITAN-I FPC were performed by the finite-element code, ANSYS [35], in order to refine and confirm the thermal-hydraulic design estimates. The blanket and shield of the TITAN-I design are not subjected to a high surface heat flux. For the first-wall channels, however, accurate descriptions of both thermal and pressure stresses are necessary. The first-wall geometries and loading conditions suggest that both the thermal and mechanical fields will exhibit significantly smaller gradients in the poloidal direction than in the radial and toroidal directions. A 2-D modeling of the cross section at the location of the extreme value of the loading in the poloidal direction, therefore, is appropriate. This approach has been used in several analyses [29,36], but the assumptions involved were not clearly indicated or were overly conservative. One possible reason for the conservatism is the virtual invariance of the temperatures and, to a lesser degree, the pressure stresses, to the assumptions for structures with large radius of curvature.

Both plane-stress and axisymmetric analyses were performed for the first-wall coolant tube. The geometry analyzed is based on a circular tube with inner diameter of 8 mm, outer diameter of 10.5 mm, and radius of curvature of 66 cm. The internal pressure is taken 10 MPa, which is the coolant pressure at the inlet. The maximum first wall temperature by ANSYS is 741°C, which is slightly lower than the prediction by the thermal-hydraulic design code presented in the previous section. The maximum equivalent pressure stress is 82 MPa in plane-stress analysis and 78 MPa in axisymmetric analysis. The corresponding values for equivalent thermal stress are respectively 98.7 MPa and 279 MPa. These stresses are shown in Fig. 12 and are within the design limits. The finite element analysis confirms the validity of the approximate design code analysis presented in the previous section.

The coolant pipes in the IBC blanket are self-supporting. A 1-D model is adequate for analyzing stress in these pipes. The maximum primary and secondary stresses in these pipes are respectively 30 MPa and 5 MPa. Because the coolant channels in the hot shield are square and rectangular in cross section, stress concentration is a major concern here. Figure 13 shows the variation of maximum pressure stress/pressure as a function of c/t, where c is the side length and t is wall thickness. The effects of corner fillet radius, r, is also illustrated in the figure. The allowable pressure stress is assumed 108 MPa, corresponding to the structure temperature at the exit of a coolant channel. The allowable pressure stress is higher at other locations. The size limit from Fig. 13 and the wall temperature limit are used to determine the dimensions of the coolant channels in the hot shield given in Table 4. Contours of equivalent primary stress in a shield coolant channel are shown in Fig. 14. The maximum stress is 40 MPa and, as expected, occurs at the corners where the stress concentration is maximum.

6. Summary and conclusions

The thermal-hydraulic design of the self-cooled first wall, blanket, and shield of the TITAN-I reactor presented here suggests that a compact and economical fusion power reactor based on the reversed-field-pinch concept of plasma confinement is possible. The main design features and improvements that have contributed to the feasibility of this design are as follow:

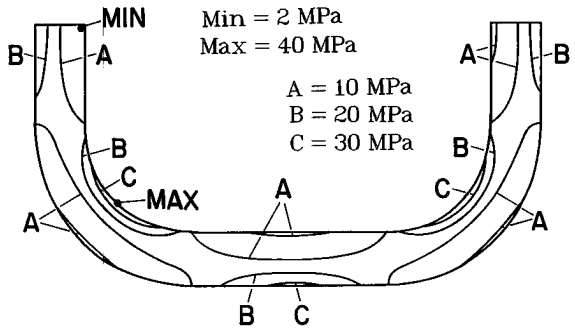

Fig. 14. Contours of the equivalent primary stresses in TITAN-I shield.

(1) Use of high-recycling divertors so that the first-wall sputtering erosion is almost negligible;
(2) Use of small-diameter, thin-walled circular tubes as coolant channels for the first wall;
(3) Use of vanadium alloy as the structural material and liquid lithium as the primary coolant;
(4) Separation of the first-wall and blanket coolant circuits;
(5) Alignment of the coolant channels with the dominant, poloidal magnetic field;
(6) Use of turbulent-flow heat transfer to remove the high heat flux on the first wall.

High-velocity (21 m/s) liquid lithium flowing in the turbulent regime cools the first wall. The thermal-hydraulic design window reveals that a maximum heat flux capability of ~ 5 MW/m^2 under the conditions of TITAN-I is possible. A separate low-velocity lithium circuit cools the IBC and hot shield. Separation of the two coolant circuits, each with different exit temperatures, led to the use of dual power cycles with a combined gross efficiency of 44%.

The use of vanadium alloy as the structural material and self-cooled, high-temperature, liquid-metal design, together with the integrated blanket coil, have contributed to the compactness of the fusion reactor core. The compactness and high power conversion efficiency have improved the economic attractiveness of TITAN-I.

The approach taken for the TITAN-I fusion power core design was to make use the best available data, to make reasonable extrapolation whenever needed and deemed achievable with further research, and to improve the present understanding in certain areas, if possible. For example, in the TITAN-I design, the heat transfer solution for plasma-facing components, i.e., first wall and divertor plates, where the heat flux is circumferentially nonuniform, has been improved.

However, several critical issues remain to be addressed. The MHD pressure-drop equations for bend, contraction, and varying magnetic field need to be substantiated by further large-scale experiments, and numerical and theoretical analyses. In MHD turbulent-flow heat transfer, experimental data should be extended to cover a wider range of the Hartmann number especially suited for the TITAN-I regime of operation (i.e., high coolant velocity in a relatively weak magnetic field). The combined effect, if any, of the parallel and perpendicular magnetic fields on flow transition and turbulent-flow heat transfer should also be investigated. The issue of liquid-metal corrosion of vanadium alloy at high velocity and temperature needs to be addressed.

The effect of nuclear volumetric heating in the coolant on film temperature drop has been neglected in the present design, as it has been in most previous fusion-reactor design studies. For high volumetric nuclear heating in the coolant, the additional film temperature drop could be appreciable [9] and should be included in future design studies.

The TITAN-I design shows that liquid-metal-cooled high-power-density RFP reactors appear feasible and attractive. However, attention is drawn to the above-mentioned inadequacies of experimental data in several areas. Further research is needed to validate the technological requirements of the TITAN-I design.

Acknowledgements

The TITAN research program is supported by the U.S. Department of Energy, Office of Fusion Energy, at University of California, Los Angeles under grant DE-FG03-86ER52126, at General Atomics under contract DE-AC03-84ER53158, at Rensselaer Polytechnic Institute under grant DE-FG02-85ER52118, and at Los Alamos National Laboratory which is operated by the University of California for the U.S. DOE under contract W-7405-ENG-36.

References

[1] F. Najmabadi et al., The TITAN reversed-field-pinch fusion reactor study, Final Report, Joint report of UCLA, GAT, LANL, and RPI, UCLA-PPG-1200 (1989); also F. Najmabadi et al., Overview of TITAN reactor study, Fusion Engrg. Des. 23 (1993) 69–80, in this issue, and S.P. Grotz et al., The TITAN-I fusion power core design, Fusion Engrg. Des. 23 (1993) 81–98, in this issue.

[2] J.H. Holroyd and J.T.D. Mitchell, Liquid lithium as coolant for tokamak fusion reactors, Culham Laboratory report CLM-R231 (1982).
[3] R.W. Moir, J.D. Lee, W.S. Neef, D.L. Jassby, D.H. Berwald et al., Feasibility study of a fission suppressed tokamak fusion breeder, Lawrence Livermore National Laboratory report UCID-20514 (1984).
[4] J.C.R. Hunt and R. Hancox, The use of liquid lithium as coolant in a toroidal fusion reactor, Part I Calculation of Pumping Power, Culham Laboratory report (1971).
[5] D.K. Sze, R. Clemmer, and E.T. Cheng, LiPb, a novel material for fusion applications, in: Proc. 4th ANS Topical Meeting on the Technology of Controlled Nuclear Fusion, King of Prussia, PA (1980).
[6] B.G. Logan et al., Mirror Advanced Reactor Study (MARS), Lawrence Livermore National Laboratory report UCRL-53563 (1984).
[7] C. Copenhaver, R.A. Krakowski, N.M. Schnurr, R.L. Miller, C.G. Bathke et al., Compact Reversed-Field-Pinch Reactor (CRFPR): Fusion-Power-Core Integration Study, Los Alamos National Laboratory report LA-10500-MS (1985).
[8] D. Steiner, R.C. Block, and B.K. Malaviya, The integrated blanket-coil concept applied to the poloidal field and blanket systems of a tokamak, Fusion Technol. 7 (1985) 66.
[9] M.Z. Hasan, Effects of nonuniform surface heat flux and uniform volumetric heating on blanket design for fusion reactors, Fusion Technol. 16 (1989) 44.
[10] W.C. Reynolds, Heat transfer to fully developed laminar flow in a circular tube with arbitrary circumferential heat flux, Trans. ASME 108 (1960).
[11] M.Z. Hasan and N.M. Ghoniem, The use of liquid-metal coolants in the thermal-hydraulic design of the first wall and blanket of high-power-density fusion reactors, University of California Los Angeles report UCLA-PPG-1086/ENG-8742 (1987).
[12] R.A. Gardner, Laminar pipe flow in a transverse magnetic field with heat transfer, Int. J. Heat and Mass Transfer 7 (1968) 1076.
[13] H. Madarame and M.S. Tillack, MHD flow in liquid-metal blankets with helical vanes, University of California Los Angeles report UCLA-ENG-8616/PPG-948 (1986).
[14] F. Issaci, N.M. Ghoniem, and I. Catton, Magnetohydrodynamic flow in a curved pipe, Phys. of Fluids 31 (1988) 65.
[15] R.A. Gardner and P.S. Lykoudis, Magneto-fluid-mechanics pipe flow in a transverse magnetic field, Part 1, Isothermal Flow, J. Fluid Mech. 47 (1971) 737.
[16] A.L. Loeffler, M. Macuilatis, and M.A. Hoffman, MHD round pipe flow experiments, U.S. Air Force report USAF-RAL 67-0236 (1967).
[17] A.L. Joumotte and C. Hirsch, Ecoulement magnetohydrodynamique en conduites, Mechanique Applique (1967) 960.
[18] S. Globe, The effect of longitudinal magnetic field on pipe flow of mercury, J. Heat Transfer 83 (1961) 445.
[19] F.W. Fraiz, The effect of strong longitudinal magnetic field on the flow of mercury in a circular tube, Ph. D. Thesis, Massachusetts Institute of Technology (1966).
[20] M.A. Hoffman, Magnetic field effect on the heat transfer of potential fusion reactor coolants, Lawrence Livermore National Laboratory report UCRL-33993 (1972).
[21] P.S. Lykoudis, Transition from laminar to turbulent flow in magneto-fluid-mechanic channels, Rev. Mod. Phys. 32 (1960) 796.
[22] H. Branover, S. Sukoriansky, G. Talmage, and E. Greenspan, Turbulence and the feasibility of self-cooled liquid metal blankets for fusion reactors, Fusion Technol. 10 (1986) 822.
[23] D.S. Kovner, E. Yu. Krasilnikov, and I.C. Panevin, Experimental study of the effects of a longitudinal magnetic field on convective heat transfer in a turbulent tube flow of conducting liquid, Magnitnaya Gidrodinamika 2 (1966) 101.
[24] R.A. Gardner and P.S. Lykoudis, Magento-fluid-mechanics pipe flow in a transverse magnetic field, Part 2, Heat transfer, J. Fluid Mech. 48 (1971) 129.
[25] E. Yu. Krasilnikov, The effect of a transverse magnetic field upon convective heat transfer in magnetohydrodynamic channel flow, Magnitnaya Gidrodinamika 1 (1965) 37.
[26] H. Schlichting, Boundary Layer Theory, 7th edition (McGraw-Hill, New York, 1979).
[27] C.C. Cheng and T.S. Lundgren, Duct flow in MHD, Z. Angew. Math. Phys. 12 (1961) 100.
[28] E.E. Sechler, Elasticity in Engineering (John Wiley & Sons, Inc., New York, 1952).
[29] R.A. Bolay and J.H. Weimer, Theory of Thermal Stress (John Wiley & Sons, Inc., New York, 1960).
[30] M.Z. Hasan, A computer code for optimum thermal-hydraulic design of the first wall and blanket of a reversed-field-pinch fusion reactor, University of California Los Angeles report UCLA-PPG-1045 (1987).
[31] M.Z. Hasan and D.K. Sze, An optimum rankine power cycle for the lithium-cooled TITAN-I reversed-field-pinch reactor, Fusion Engrg. Des. 9 (1989) 425.
[32] L.C. Fuller and T.K. Stovall, User's Manual for PRESTO: a computer code for the performance of regenerative superheated steam-turbine cycles, Oak Ridge National Laboratory report ORNL-5547, NASA CR-159540 (1975).
[33] I.J. Karassik, W.C. Krutzsch, W.H. Fraser, and J.P. Messina (Eds.), Pump Handbook (McGraw-Hill, New York, 1976).
[34] L.G. Hays, Corrosion of niobium–1% zirconium alloy and yttria by lithium at high flow velocities, NASA-JPL Technical report 32–1233 (1967).
[35] G.J. DeSalvo and J.A. Swanson, ANSYS User's Manual (Swanson Analysis Systems, Inc., 1979).
[36] D.L. Smith, G.D. Morgan, M.A. Abdou, C.C. Baker, J.D. Gordon et al., Blanket comparison and selection study – Final Report, Argonne National Laboratory report ANL/FPP-84-1 (1984).